Applied Catalysis B: Environmental 183 (2016) 18–27

Contents lists available at ScienceDirect

Applied Catalysis B: Environmental

journal homepage: www.elsevier.com/locate/apcatb

Acetone and ethanol vapor oxidation via negative atmospheric corona discharge over titania-based catalysts

Mikhail N. Lyulyukin[a,b,c,*], Alexey S. Besov[a,b], Alexander V. Vorontsov[a]

[a] Boreskov Institute of Catalysis, Pr. Ak. Lavrentyeva 5, Novosibirsk 630090, Russia
[b] Novosibirsk State University, st. Pirogova 2, Novosibirsk 630090, Russia
[c] Research and Educational Center for Energy Efficient Catalysis in Novosibirsk State University, st. Pirogova 2, Novosibirsk 630090, Russia

ARTICLE INFO

Article history:
Received 6 July 2015
Received in revised form
24 September 2015
Accepted 12 October 2015
Available online 23 October 2015

Keywords:
NTP
Post-plasma catalysis
VOCs
Titanium dioxide
Copper oxide
Manganese oxide

ABSTRACT

The paper is devoted to the oxidation of acetone and ethanol vapors by means of an optimized negative atmospheric corona discharge combined with TiO_2-based catalysts located in a post-plasma position. A series of studied samples includes CuO-MnO_2/TiO_2, CuO/TiO_2 and MnO_2/TiO_2 with 3 wt% of copper oxide and 6.8 wt% of manganese oxide. Experiments were performed at room temperature in a closed 404-L chamber with a ~0.9-L active plasma region. It was shown that the use of the catalysts can provide a significant reduction in the concentrations of ozone and oxidation byproducts and a three-fold increased conversion of the reactants. It was unexpectedly found that copper oxide, as an active agent, did not significantly change the effect of post-plasma-located TiO_2. The manganese-containing sample was found to be the best catalyst at the conditions considered. The presence of this catalyst in the post-plasma position inhibits the formation of unwanted products (O_3 and CO) and promotes the deep oxidation of acetone and ethanol with increased selectivity toward CO_2.

1. Introduction

Population of the planet is faced with the global problem of environmental pollution. Various industrial and agricultural processes are the common source of air pollution, and their existence is a problem for human health and the environment in general. A great part of pollutants are Volatile Organic Compounds (VOCs). This category includes most solvent thinners, degreasers, cleaners, some lubricants, and liquid fuels [1]. Some VOCs are dangerous to human health and harm the environment. A number of control technologies are used to alleviate the pollution problem. They are basically divided into two groups: destruction and recovery methods. Recovery is a relatively good method for a wide range of purification tasks. However, its main drawback is the need for the regeneration of sorbent materials. In contrast, destruction-based methods do not have this disadvantage because pollutants are transformed into mostly harmless inorganic compounds.

One promising destruction-based method has recently gained a lot of attention. It is the oxidation of VOCs by means of a combination of an atmospheric Non-Thermal Plasma discharge (NTP oxidation) with catalysts. Generation of NTP in air is a well-known method of air purification [2,3], which is characterized by relatively low capital and operational costs. However, it has drawbacks such as poor energy efficiency and generation of ozone and other harmful by-products, which decreases the selectivity of oxidation of VOCs toward CO_2. A combination of the NTP with catalysis may possibly reduce the negative effects of the NTP and improve the performance of purification systems.

There are a number of reviews on the treatment of VOCs using a combined plasma-catalytic oxidation [4–7]. The combination of plasma with catalysts was found to be reasonable because plasma produces many active species like electrons, ions, free radicals, excited species, and photons, and all of them can participate directly or indirectly in oxidative reactions over a catalyst. Combined plasma-catalytic systems can be divided into single-stage systems, also called In-Plasma Catalysis (IPC) or Plasma-Driven Catalysis (PDC), and two-stage systems, also called Post-Plasma Catalysis (PPC) or Plasma-Enhanced Catalysis (PEC). Systems of both types have their own advantages and limitations. The IPC provides a combination of simultaneous gas-phase and surface reactions. A catalyst located inside the plasma region can also affect the discharge. Porous catalytic materials placed into an IPC system may enhance selectivity toward the formation of CO_2 [8]. However, IPC systems are difficult to optimize. Besides, because of technical limitations, they are based mostly on the Dielectric Barrier Discharge (DBD) [9], which is very difficult to scale. In contrast, PPC systems are more capable of optimization because both the

* Corresponding author at: Boreskov Institute of Catalysis, Pr. Ak. Lavrentyeva 5, Novosibirsk 630090, Russia.
E-mail addresses: lyulyukin@catalysis.ru, axim@ngs.ru (M.N. Lyulyukin).

http://dx.doi.org/10.1016/j.apcatb.2015.10.025
0926-3373/

discharge and the catalyst can be varied independently. In the PPC oxidation, plasma promotes a partial conversion of pollutants and a generation of ozone and other active species, which can enhance the oxidation to CO_2 over a post-plasma catalyst.

A variety of catalytic materials can be used for the PPC at room or elevated temperatures. For example, the oxidation of ethanol and acetone with ozone has been performed at 300–573 K over manganese oxide supported on alumina or on silica [10,11]. It was shown that ethanol reacted with O_3 at a lower temperature than with O_2, and with a lower activation energy. The oxidation of acetone with ozone was also highly accelerated on both catalysts. The only detected carbon-containing product was CO_2. Another example of the PPC is the use of a commercial ozone decomposition catalyst ($CuO + MnO_2$)/TiO_2 for toluene removal. It was shown that the application of this catalyst improved the removal efficiency up to 40 times [12]. In addition, the destruction of ozone over a MnO_2 catalyst was found to enhance the destruction of benzene vapors [13].

In our earlier research, we investigated the oxidation of acetone and ethanol vapors in an atmospheric pressure corona discharge (CD) at a near room temperature [14,15]. For generating the NTP, we used a double-wire-to-plane discharge gap geometry and found the optimal wire diameter, polarity and power input that provided the highest cost efficiency. However, we have also faced such well-known problems of air purification with the CD as relatively low energy efficiency and the formation of oxidation by-products and ozone.

The present paper demonstrates our results of placing catalysts CuO-MnO_2/TiO_2, CuO/TiO_2, and MnO_2/TiO_2 downstream the CD unit, i.e., in the post-plasma position. Such a combination of the NTP and catalysis can help to reduce the drawbacks of plasma application and improve the total efficiency of the system. The samples were compared to determine the optimal composition of a post-plasma catalyst for the purpose of air purification. A large free-air volume (i.e., the volume not exposed to plasma) is the main distinction of our experimental setup. In our opinion, this approach is closer to the conditions of the practical application of air purification techniques.

2. Experimental

2.1. Chemicals

High purity acetone, 96% ethanol, and room air at atmospheric pressure with relative humidity about 45–50% were used in the experiments without preliminary cleaning.

2.2. Experimental setup

The used experimental setup is very similar to that described in detail previously [14,15]. A scheme of the experimental setup is demonstrated in Fig. 1A. A stack of double-wire-to-plane discharge units was placed inside a 404-L Plexiglas chamber connected to an FTIR analysis system. The most efficient regime of the CD was selected on the basis of our previous results [15]: the diameter of corona wire was 0.8 mm, the corona current was fixed at 1 mA, and the corresponding voltage across the discharge gap was about 13 kV, which corresponds to the discharge power of 13 W.

To create a PPC system, a mesh support with a deposited catalyst (Fig. 1B) was located in the post- plasma position (downstream the corona discharge unit at the distance 350 mm). The air flow rate was 135 m^3/h in presence of catalytic support. The mass of the catalyst was about 2.5 g. The support with the size of 13.5 cm × 14.5 cm was made of fiberglass mesh impregnated with aqueous α-Al_2O_3 and an inorganic binder based on γ- Al_2O_3.

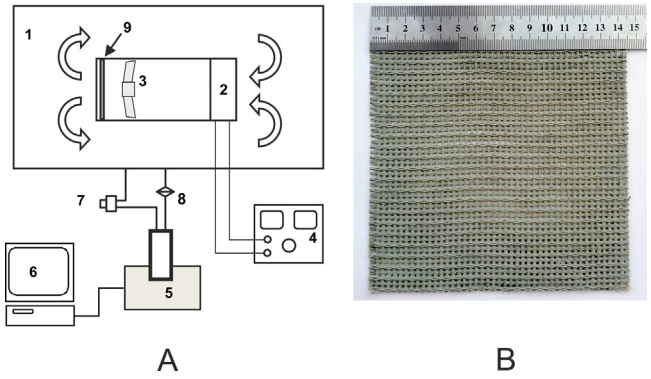

Fig. 1. (A) Scheme of the experimental setup: (1) test chamber (404 L), (2) corona discharge unit, (3) fan, (4) high voltage DC power supply source, (5) FTIR spectrophotometer Vector 22 (Bruker) with multipass gas cell, (6) computer, (7) membrane pump, (8) 0.2 μm filter, (9) fiberglass mesh with deposited catalyst; (B) photo of the fiberglass mesh with deposited MnO_2/TiO_2 sample.

In every experiment, the initial vapor–air mixture contained 200 ppm of a studied substrate. The mixture was purged through the cell using plastic tubing and a 0.2-μm air filter under the action of a membrane pump. Concentrations of organic vapors, O_3, CO, and CO_2 in the chamber were measured with an FTIR spectrophotometer Vector 22 (Bruker) equipped with a multipass gas cell of 0.7 L volume. The FTIR spectrophotometer allowed continuous measuring of concentrations of reagents and products. The FTIR spectra were recorded in the wavenumber range 450–4000 cm^{-1} with the resolution of 1 cm^{-1} at 30 s intervals. Each spectrum represents an average of 10 scans. Concentrations of organics and CO_2 were calculated from the areas of absorption bands in the IR spectra. The rates of changes in substance concentrations were calculated by using a linear approximation. Original software Difference was used for the processing of numerous spectra. Calculations were based on a novel method of spectral subtraction of gas-phase FTIR spectra by minimizing the spectrum length [16].

2.3. Catalyst preparation

TiO_2 Hombifine N (S_{BET} = 350 m^2/g) was used as a basis for preparing the catalysts. The deposition was performed by the impregnation method. Copper and manganese nitrates ($Cu(NO_3)_2$ and $Mn(NO_3)_2$) were used as precursors for copper and manganese oxides. TiO_2 was impregnated with a 0.5-M aqueous solution of precursors. Then, the mixture was dried at 120 °C and calcined at 500 °C for 5 h. The aqueous solution was deposited on the mesh after cooling and grinding the catalyst.

The list of synthesized catalysts with the targeted oxide content (by weight) is shown in Table 1. The series of samples includes pure TiO_2 Hombifine N and five samples of TiO_2 modified with CuO and/or MnO_2. The whole set of samples allows one to reveal a number of correlations and to elucidate the role of an added oxide. Sample 1 is a reference sample. Samples 2 and 3 would show the effect of each additive separately. Samples 4–6 would give information about the dependence of sample properties on the order of additive deposition. Additional experiments without any catalyst were carried out for both acetone and ethanol to make a comparison with an ordinary NTP oxidation.

The catalysts were characterized by X-Ray Diffraction analysis (XRD), X-Ray Photoelectron Spectroscopy (XPS), and Transmission Electron Microscopy (TEM). The XRD analysis of the samples was carried out with a Bruker D8 Advance with the copper irradiation (wavelength 1.5418 Å). The XPS analysis of some samples (3, 5, 6 and sample 5 after use) was performed using a SPECS apparatus. The spectrometer was equipped with a semispherical analyzer

Table 1
List of synthesized catalysts and the targeted oxide content.

No.	Catalyst	Targeted content	Features	S_{BET} (m^2/g)
1	TiO_2	–	–	350
2	CuO/TiO_2	3% CuO	–	117
3	MnO_2/TiO_2	6.8% MnO_2	–	111
4	v1. $CuOMnO_2/TiO_2$	3% CuO, 6.8% MnO_2	CuO deposited first	103
5	v2. $CuOMnO_2/TiO_2$	3% CuO, 6.8% MnO_2	MnO_2 deposited first	93
6	v3. $CuOMnO_2/TiO_2$	3% CuO, 6.8% MnO_2	Simultaneous deposition	100

PHOIBOS-150 and an X-ray source of the characteristic radiation XR-50 M with a dual Al/Ag anode. Monochromated radiation Al Kα ($h\nu$ = 1486.74 эВ) was used to record the spectra. Binding energies E_{bind} were calibrated using the Ti2p line of titanium (E_{bind} = 459.00 eV) as an internal standard. Relative concentrations of the elements were determined on the basis of integrated intensities of corresponding XPS lines [17]. The decomposition of the spectra into individual components was used for a detailed analysis. The experimental curves were decomposed into a number of lines corresponding to the photoemission of electrons from the atoms in different chemical environments after background subtraction using the Shirley method [18]. The data were processed by using the CasaXPS software [19]. XPS line shapes were approximated with a product of symmetrical Gaussian and Lorentz functions. High-resolution Transmission Electron Microscopy (TEM) micrographs were obtained with a JEM-2010 (JEOL, Japan) instrument with the lattice resolution 0.14 nm and accelerating voltage 200 kV. The samples for the TEM study were prepared by ultrasonic dispersing in ethanol and subsequent deposition of the suspension onto a perforated carbon film supported on an alumina grid. Local elemental analysis was performed by the EDX method using an Energy-dispersive X-ray Phoenix Spectrometer equipped with a Si (Li) detector with the energy resolution of about 130 eV.

3. Results and discussion

3.1. Catalyst characterization

XRD patterns of the samples are presented in Fig. 2. As seen from the picture, TiO_2 is in the anatase phase in each of the catalysts. In addition, sample 5 exhibits low-intense peaks at 28.7 and 56.6° (shown with circles in Fig. 2), which indicate that this sample contains slight amounts of MnO_2 pyrolusite as a separate phase. The size of the coherent scattering region obtained from peak widths is 10–20 nm for all the samples.

XPS spectra of the investigated catalysts include lines corresponding to Ti, Mn, Cu, O, and C. In preliminary experiments, all

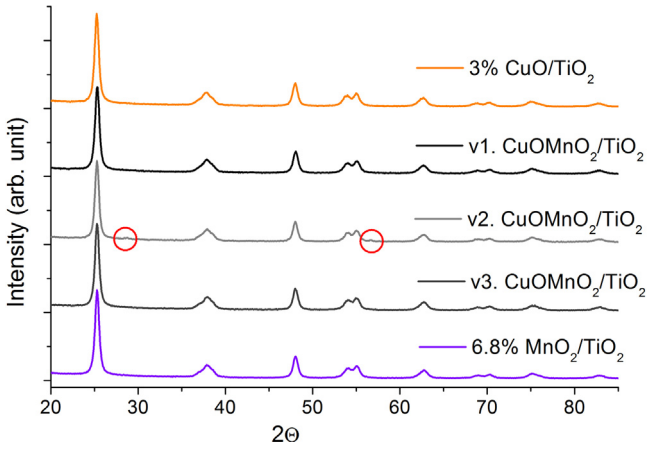

Fig. 2. XRD patterns of studied catalysts.

Table 2
Relative atomic concentrations of the elements in the surface layer of samples.

No.	Sample	[Mn]/[Ti]	[Cu]/[Ti]	[O]/[Ti]
3	MnO_2/TiO_2	0.034	–	2.65
5	v2. $CuOMnO_2/TiO_2$	0.050	0.054	2.55
6	v3. $CuOMnO_2/TiO_2$	0.054	0.054	2.60
5*	v2. $CuOMnO_2/TiO_2$ after use	0.061	0.062	2.74

($CuO + MnO_2$)/TiO_2 samples demonstrated similar catalytic properties, which apparently indicates that they also have similar structural characteristics. To confirm this hypothesis, we studied the structures of samples Nos. 5 and 6. Table 2 shows the composition of several catalysts. As seen from the table, ratios [Mn]/[Ti] and [Cu]/[Ti] vary in a narrow range of 0.05–0.06 for the copper-containing catalysts. The amount of manganese in sample 3 was 6.8% as well as in samples 5 and 6 but the ratio [Mn]/[Ti] was 0.034 instead of 0.050–0.060. This significant difference in surface concentrations can be caused by the fact that the absence/presence of copper oxide leads to the enlargement/reduction of manganese oxide particles. It is possible that in sample 3, manganese oxide is in the form of large particles.

There are two peaks $Ti2p_{3/2}$ and $Ti2p_{1/2}$ in Ti2p spectra. The $Ti2p_{3/2}$ line has a symmetrical shape with the FWHM = 1.5 eV. The $Ti2p_{3/2}$ binding energy for TiO_2 is in the range of 458.7–459.2 eV, and the corresponding values for the Ti^{3+} state are about 456.2 eV. Therefore, titanium in the studied samples is mostly in the Ti^{4+} state in the structure of TiO_2. The $Ti2p_{3/2}$ line with E_{bind} = 459.0 eV was used as an internal standard with taking into account the effect of sample charging. An additional slight doublet with the $Ti2p_{3/2}$ binding energy of 457.9 eV observed in catalyst 6 can be attributed to titanium in the Ti^{3+} state.

Table 3 represents the binding energy of elements in some of the catalysts studied. Fig. 3A shows the Mn2p spectra of investigated catalysts. The spectrum is a $Mn2p_{3/2}$–$Mn2p_{1/2}$ doublet with the integral intensities of the lines relating as 2:1. The corresponding spin-orbit splitting is 11.8 eV. The asymmetrical shape of the lines is determined by many-electron processes. The binding energies of $Mn2p_{3/2}$ are in the ranges 640.4–641.7, 641.5–641.9, and 642.2–642.6 eV for MnO, Mn_2O_3, and MnO_2, respectively [20,21]. Therefore, the detected value of the $Mn2p_{3/2}$ binding energy 642.2 ± 0.2 eV (Table 3) indicates that manganese in our samples exists in the Mn^{4+} state. The additional peak at 650 eV in catalysts with copper refers to the Cu*LMM* Auger line.

Fig. 3B shows the $Cu2p_{3/2}$ spectra of investigated catalysts. There are lines at 942 and 944 eV in addition to the intense lines at 934.6 ± 0.2 eV. These additional lines are so-called "shake up" satellites that are usually observed in spectra of Cu^{2+} compounds. In contrast, these satellites are missing in spectra of metallic copper and Cu^{1+} compounds. The $Cu2p_{3/2}$ binding energy for metallic copper and Cu_2O are in the ranges of 932.5– 932.7 and 932.4–932.9 eV, whereas the $Cu2p_{3/2}$ binding energy of CuO is in the range of 933.6–934.1 eV. Therefore, copper in these catalysts exists mainly in the Cu^{2+} state.

Four samples were analyzed by TEM. The most frequently observed periodic lattices correspond to 101 reflection of the TiO_2

Table 3
$Mn2p_{3/2}$, $Cu2p_{3/2}$, O1s, and C1s binding energies. Calibration via the Ti2p line with E_{bind} = 459.0 eV.

No.	Sample	$Mn2p_{3/2}$	$Cu2p_{3/2}$	O1s	C1s
3	MnO_2/TiO_2	641.95	–	530.25 (86.9) 532.26 (13.1)	285.32
5	v2. $CuOMnO_2/TiO_2$	642.21	934.40	530.34 (90.4) 532.26 (9.6)	285.32
6	v3. $CuOMnO_2/TiO_2$	642.18	934.60	530.29 (95.0) 532.51 (5.0)	285.21
5*	v2. $CuOMnO_2/TiO_2$ after use	642.26	934.77	530.27 (87.4) 532.31 (12.6)	285.32

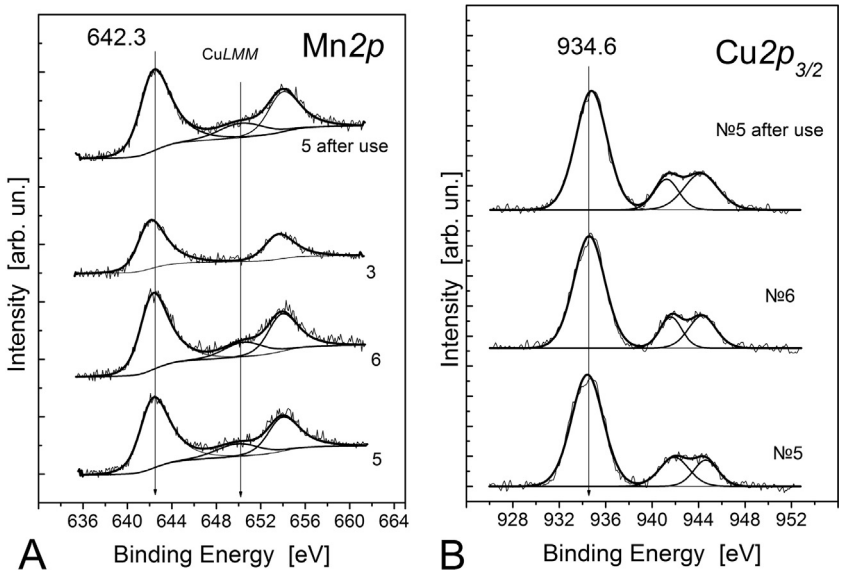

Fig. 3. Mn2p (A) and $Cu2p_{3/2}$ (B) spectra of investigated catalysts. The spectra are normalized to the integrated intensity of the corresponding $Ti2p_{3/2}$ spectra.

anatase phase with the parameter 0.352–0.359 nm. According to EDX data, Mn and Cu are present at all the analysis points of catalysts 5, 6, and catalyst 5 after use (Figs. 4–6 , respectively). The content of manganese is about 3–7 at.% in all the samples and the content copper is 3–4 at.%. These values are in good agreement with the results of the XPS analysis. No change in the content was observed for the used sample. Individual particles of MnO_2 were found only in fresh sample 5. There were also found a small portion of Mn_3O_4 and Mn_2O_3 particles. However, there was no evidence of their existence in sample 5 after its use. Individual particles of copper oxide were not found in any sample.

Individual particles of MnO_2 were not found in sample 3, but Mn atoms were detected in every tested point of this catalyst (Fig. 7). According to EDX analysis, the average content of Mn on the surface of this sample is about 2–3 at.%. However, there were also a number of particles with a content of Mn about 5%.

3.2. Oxidation with post-plasma located TiO_2

Figs. 8 and 9 show changes in the concentrations of initial substrates, organic intermediate products of oxidation, CO, CO_2, and ozone during the experiment. The corona discharge unit was switched on after the substrate concentration reached a pseudo-stationary level. This moment is marked with the first vertical line. The corona was switched off after 150 min as indicated with the second vertical line. Symbols in the pictures show every tenth experimental point for the clarity of presentation.

The substrate concentrations start to decrease rapidly after the beginning of the discharge. CO_2, CO, ozone, and such organic gaseous intermediates as acetaldehyde, formaldehyde, and acetic acid appear in the air mixture as a result of chemical transformations. The concentration of ozone continuously increases while the discharge glows but gradually decreases after turning it off. Concentrations of organic products were changing even after the plasma treatment. It shows that some chemical reactions proceed “in the dark”, i.e., involving only accumulated ozone.

The initial rates of consumption of substrate vapors and the rates measured just before the end of the corona discharge (i.e., final rates) are presented in Table 4. The decomposition rates that were detected after the plasma treatment are presented there as well. These rates were calculated to compare the interaction of a test compound with accumulated ozone in the presence and in the absence of a catalyst. The calculations were made by linear approximation of 40 experimental points (20 min). This comparison is of a special interest because the interaction of acetone and ozone in experiments on non-catalytic NTP oxidation of acetone did not give a significant impact on the overall decomposition rate.

Selectivity toward CO_2 and CO is often used for the analysis of VOC removal. It is an important factor for the characterization of NTP oxidation because a poor selectivity means a low efficiency of the technique. The selectivities were calculated by the following well-known formulas [22]

$$S_{CO_2}(\%) = \frac{[CO_2]_{final} - [CO_2]_{initial}}{3([Acetone]_{initial} - [Acetone]_{final})} \times 100\%,$$

$$S_{CO_2}(\%) = \frac{[CO_2]_{final} - [CO_2]_{initial}}{2([Ethanol]_{initial} - [Ethanol]_{final})} \times 100\%,$$

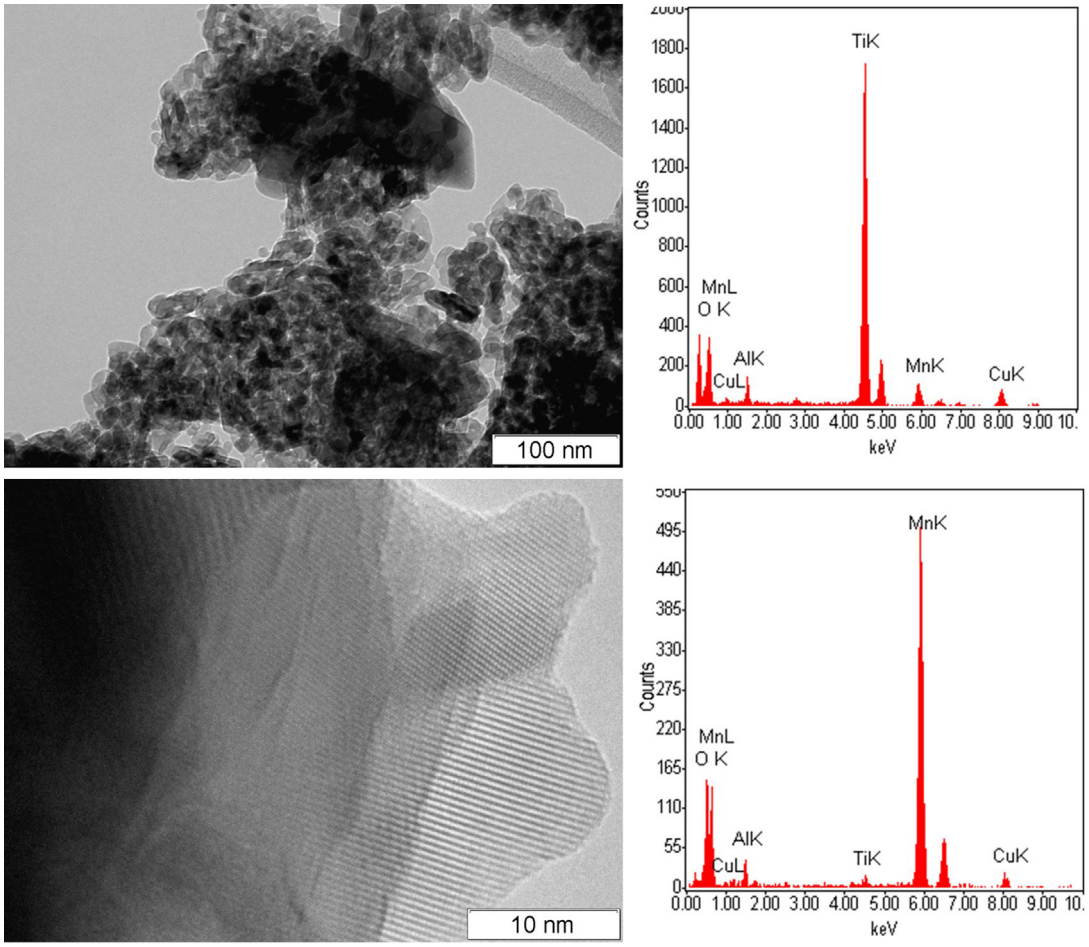

Fig. 4. TEM micrographs of catalyst 5 (v2. $CuOMnO_2/TiO_2$).

Table 4
Non-catalytic and PPC oxidation of acetone and ethanol.

	Acetone		Ethanol	
	No catalyst	TiO_2	No catalyst	TiO_2
Initial consumption rate (ppm/min)	0.24	0.54	0.81	0.42
Final consumption rate (ppm/min)	0.15	0.36	0.74	0.37
Consumption rate with ozone(ppm/min)	0.06	0.11	0.31	0.15
Substrate conversion (%)	19	48	75	58
CO selectivity (%)	51	9	27	7
CO_2 selectivity (%)	40	49	45	47
Ozone consumption rate (ppm/min)	0.06	0.14	0.16	0.17
Ozone max. concentration (ppm)	72.8	59.8	76.8	44.2

and

$$S_{CO}(\%) = \frac{[CO]_{final} - [CO]_{initial}}{3([Acetone]_{initial} - [Acetone]_{final})} \times 100\%,$$

$$S_{CO}(\%) = \frac{[CO]_{final} - [CO]_{initial}}{2([Ethanol]_{initial} - [Ethanol]_{final})} \times 100\%,$$

Factors in the denominator mean the number of molecules of carbon oxides released from a single molecule of the initial substance. The calculations were made for the moments at the end of the corona discharge with taking into account the amount of adsorbed initial substances.

Because the tested samples are considered to be ozone degradation catalysts, it is necessary to compare their activities in the ozone decomposition. For this purpose, two parameters have been selected: the maximum concentration of ozone during the oxidation and the rate of ozone degradation immediately after the plasma treatment. Both parameters are presented in Table 4 for the non-catalytic NTP oxidation and for the PPC oxidation of acetone and ethanol over TiO_2.

As seen from Table 4, the PPC oxidation with pure TiO_2 results in an increase in the rate of ozone degradation and in a decrease in the maximum concentration of ozone in comparison with non-catalytic oxidation. This is a result of the TiO_2 catalytic effect. Because the decomposition of ozone requires participation of a third body M, the larger number of active M will increase the decomposition rate according to the following equations:

$$O_3 + M \rightarrow O + O_2 + M,$$

$$O_3 + O \rightarrow 2O_2.$$

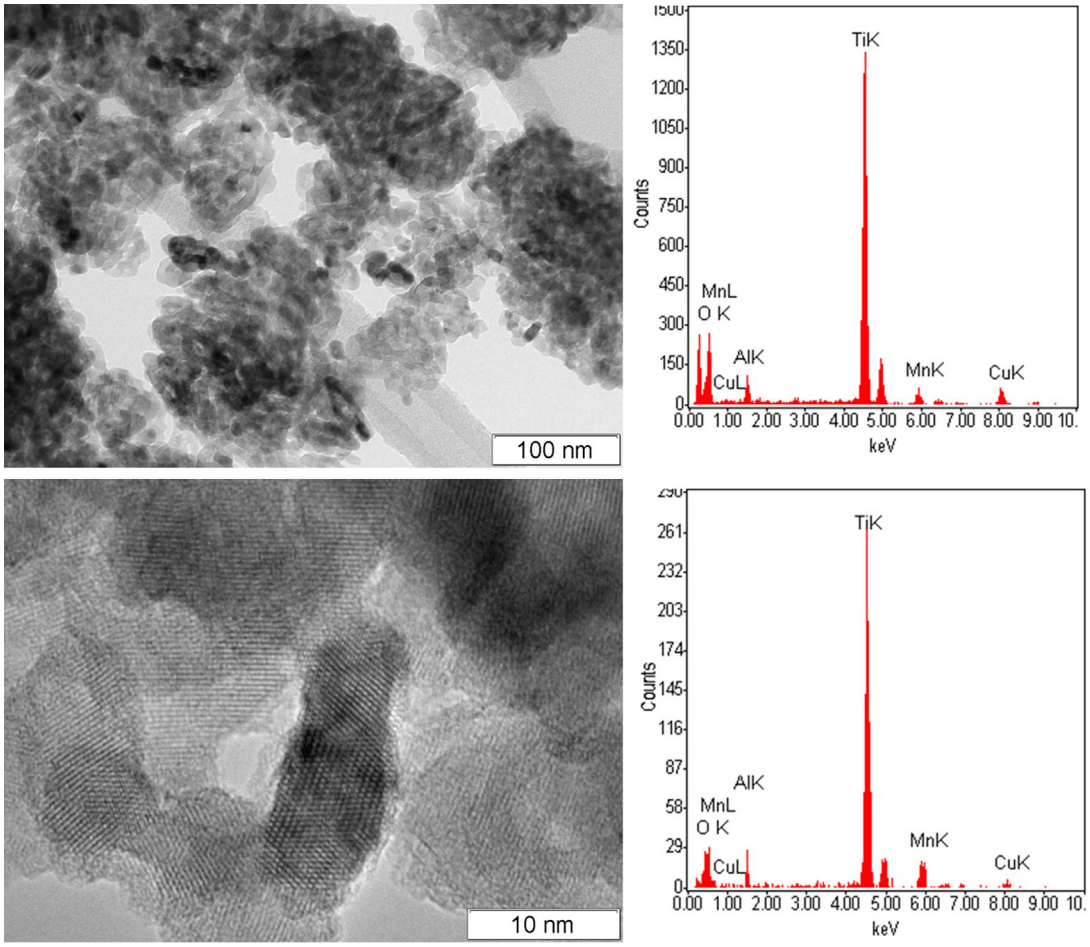

Fig. 5. TEM micrographs of catalyst 6 (v3. $CuOMnO_2/TiO_2$).

In the presence of a surface, the role of M is played by surface sites [23] (denoted with an asterisk)

$$O_3 + * \rightarrow O* + O_2*,$$

$$O_3 + O* \rightarrow O_2* + O_2,$$

$$O_2* \rightarrow * + O_2.$$

The resulting additional O^* could possibly react with the adsorbed substances and with ozone [11]. In our case, these substances (acetone and ethanol) are designated as VOC.

$$VOC + * \rightarrow VOC*,$$

$$VOC* + O* \rightarrow \text{products}.$$

Post-plasma located TiO_2 caused a twofold increase in the initial and final rates of acetone consumption (Table 4). The substrate conversion (calculated from the values after switching off the plasma) has also increased 2.5 times, which is obviously a positive change in the acetone oxidation. The selectivity toward the formation of carbon oxides significantly changed as well: with the use of TiO_2, CO_2 became a predominant product. In the case of ethanol (Fig. 9), the use of TiO_2 resulted in adsorption of almost half of the initial amount of the substrate (without a catalyst, the initial concentration of a substrate was 200 ppm). This led to a twofold decrease in the observed consumption rates due to desorption of adsorbed ethanol from the catalyst surface. Despite the decrease in the consumption rates, the selectivity toward CO_2 increased. The great increase in the selectivity toward CO_2 may be attributed to a faster formation of CO_2 from such intermediates of ethanol oxidation as acetaldehyde and formaldehyde in oxidation on the surface of catalyst. The selectivity toward CO decreased for the same reasons.

3.3. Oxidation with post-plasma located $CuOMnO_2/TiO_2$

3.3.1. Acetone oxidation

Table 5 shows the results of acetone oxidation with different variants of the $CuOMnO_2/TiO_2$ post-plasma catalyst. With the use of sample 4 (when CuO was deposited before MnO_2), the initial consumption rate remained at the level of the initial rate obtained with pure TiO_2 (Table 4). The final decomposition rate with this catalyst was slightly higher, and the consumption after turning off the discharge was twice faster than that with pure TiO_2. This sample was also slightly more active in the ozone decomposition: the degradation rate and maximum concentration changed by a quarter of the values measured for TiO_2. Samples v2 and v3 were less active in the consumption of acetone with accumulated ozone than the sample v1. In addition, 2nd and 3rd variants of $CuOMnO_2/TiO_2$ are very close to each other in their effect on the experimental process. Differences between them are negligible when compared with the sample v1.

Acetone consumption rates with CuO/TiO_2 (sample 2) are similar to those obtained with TiO_2: initial and final rates are about twice as much as the rates obtained in the non-catalytic NTP oxidation (Table 4). The rate of acetone consumption with accumulated ozone is almost the same as that for the non-catalytic oxidation with NTP. Thus, the doping of TiO_2 with copper oxide

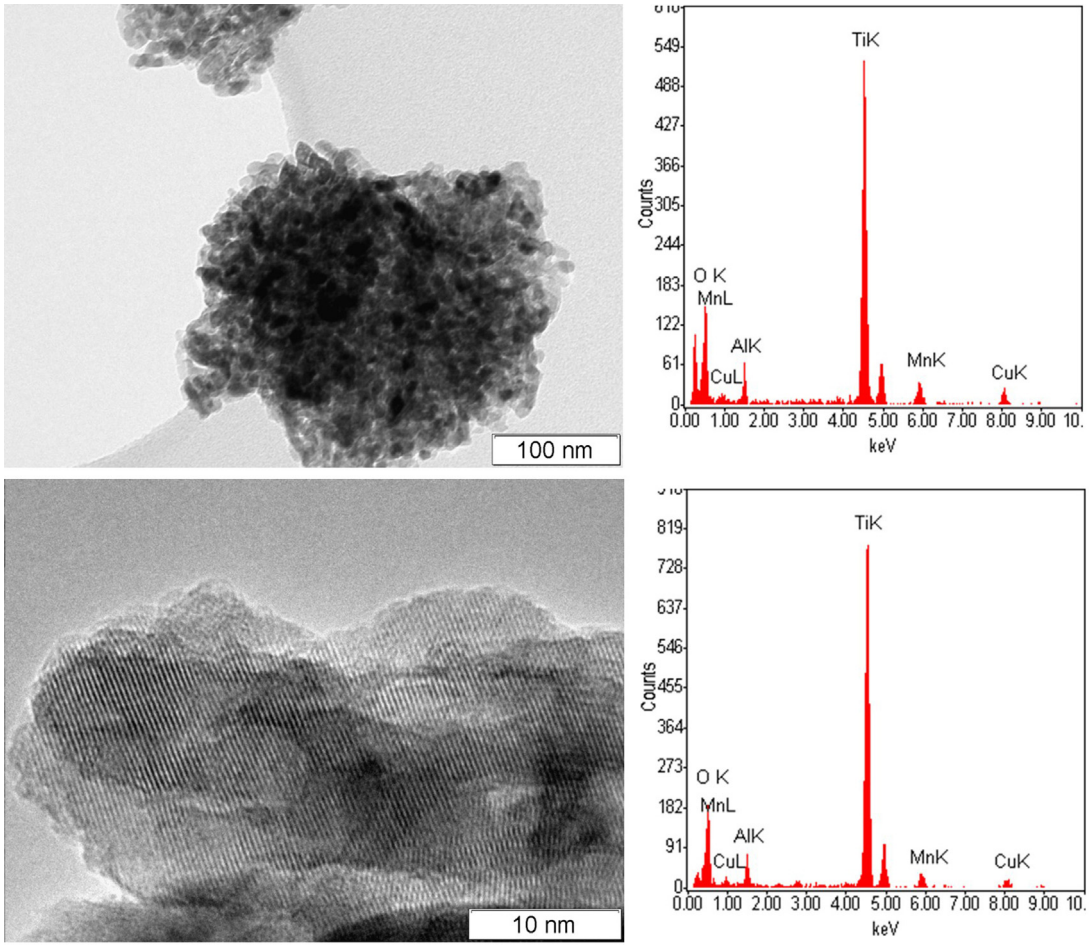

Fig. 6. TEM micrographs of catalyst 5 (v2. $CuOMnO_2/TiO_2$) after use.

Table 5
Oxidation of acetone with different post-plasma catalysts.

	$CuOMnO_2/TiO_2$			CuO/TiO_2	MnO_2/TiO_2
	v1.	v2.	v3.		
Initial consumption rate (ppm/min)	0.58	0.99	1.07	0.58	0.77
Final consumption rate (ppm/min)	0.48	0.41	0.38	0.30	0.52
Consumption rate with ozone (ppm/min)	0.25	0.18	0.18	0.07	0.32
Substrate conversion (%)	55	62	67	37	70
CO selectivity (%)	18	14	12	21	9
CO_2 selectivity (%)	52	51	49	46	64
Ozone consumption rate (ppm/min)	0.21	0.18	0.18	0.12	0.29
Ozone max. concentration (ppm)	36.2	48.2	45.9	75.6	23.7

did not enhance decomposition and oxidation properties of the catalyst.

All the manganese-containing samples are noticeably different from the other catalysts. The rates of ozone consumption are higher, and maximum ozone concentrations are lower for these samples. All the variants of $CuOMnO_2/TiO_2$ show a similar behavior in the ozone decomposition, with a slight difference of the variant v1. The highest activity in the decomposition of ozone was observed for the MnO_2/TiO_2 sample. Moreover, decomposition of acetone in the reaction with ozone proceeds 3 times faster with this sample than with pure titanium dioxide.

Selectivity toward CO_2 is in the range of 45–52% for most samples. Selectivity toward toxic CO became lower with the use of every tested sample compared with the non-catalytic NTP treatment. The most effective sample is MnO_2/TiO_2: selectivity toward carbon dioxide over this sample achieves 64%, while the selectivity toward CO is about 9%, which is the lowest value obtained with the doped samples. The kinetic curves of substances obtained during the acetone oxidation with this catalyst are shown in Fig. 10.

3.3.2. *Ethanol oxidation*

The results of plasma-catalytic oxidation of ethanol are presented in Table 6. The vapor concentration of ethanol decreased so rapidly with the use of all the MnO_2-containing samples that its concentration in the gas mixture fell below the detection level before the stop of discharge operation. Therefore, Table 6 reports the maximal linear consumption rates, which were observed from 60 to 90 min (Fig. 11).

It can be seen from the data that the order of oxide deposition did not affect the oxidation of ethanol. The maximum degradation

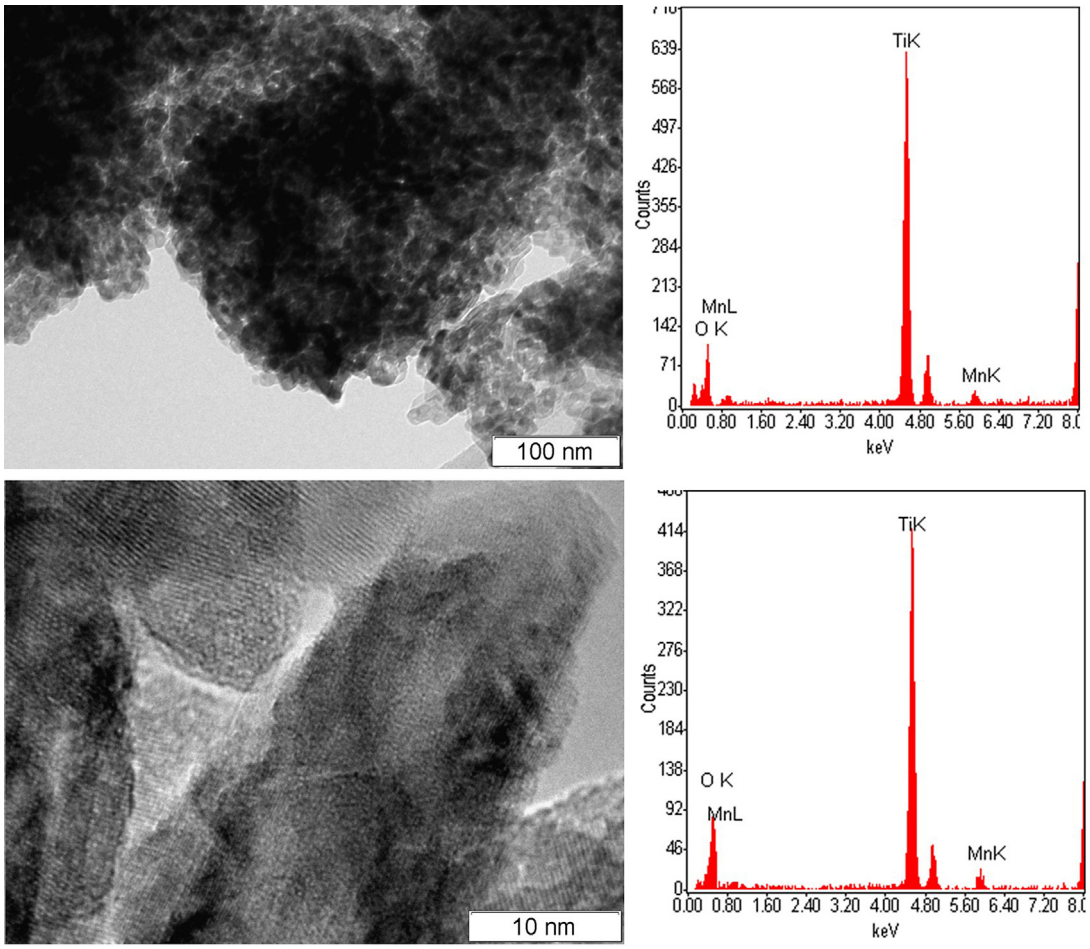

Fig. 7. TEM micrographs of catalyst 3 (6.8% MnO_2/TiO_2).

Table 6
Oxidation of ethanol with different post-plasma catalysts.

	$CuOMnO_2/TiO_2$			CuO/TiO_2	MnO_2/TiO_2
	v1.	v2.	v3.		
Maximum consumption rate (ppm/min)	2.40	2.38	2.48	0.63	2.66
Substrate conversion (%)	~100	~100	~100	70	~100
CO selectivity (%)	16	14	14	18	13
CO_2 selectivity (%)	40	46	43	45	54
Ozone consumption rate (ppm/min)	0.14	0.14	0.14	0.16	0.26
Ozone max. concentration (ppm)	47.5	40.4	43.0	66.0	27.5

rates were almost equal for all the $CuOMnO_2/TiO_2$ samples. Selectivities toward carbon oxides were also within a narrow range. Moreover, the activity of these samples in the decomposition of ozone is practically equal to the activity of pure TiO_2. The rate of decomposition of ethanol vapors with the use of $CuOMnO_2/TiO_2$ is 6 times higher than that with the use of pure TiO_2. Therefore, the substrate conversion was almost complete in these cases, and the gas-phase concentration of ethanol was below the detection level when the discharge was switched off. The selectivity toward carbon dioxide of about 50% means that only half of initial ethanol was successfully mineralized despite the high consumption rates.

The consumption rate of ethanol with the CuO/TiO_2 sample was 1.5 times higher than that with the TiO_2 sample. The selectivities toward carbon oxide with all copper-containing samples were still better than the selectivities obtained during the non-catalytic NTP oxidation but worse than the selectivities achieved with pure TiO_2.

The total conversion of ethanol to carbon oxides with the MnO_2/TiO_2 sample was almost 100%. However, the selectivity toward carbon monoxide of 13% was still too high for practical applications. Besides, this sample is sufficiently different from the others in the accumulation and decomposition of ozone (Tables 5 and 6). However, the effect of manganese oxide addition is much more noticeable in the oxidation of ethanol. The decomposition rate of ethanol vapors over the MnO_2/TiO_2 sample was also higher than that over the other samples.

Fig. 11 shows the kinetic curves of substances observed during the oxidation of ethanol vapors with the sample MnO_2/TiO_2. Acetaldehyde, formaldehyde, and acetic acid reach their maximums during the discharge. This shows their intermediate role in the ethanol oxidation. The maximum concentration of formic acid of about 2 ppm was observed in 10 min after the maximum of formaldehyde. The kinetic curves for formic acid are not presented in the figures because the experimental error of its detection is about 1 ppm (half of the maximum value). Taking into account the sequence of the intermediate maximums, we may propose

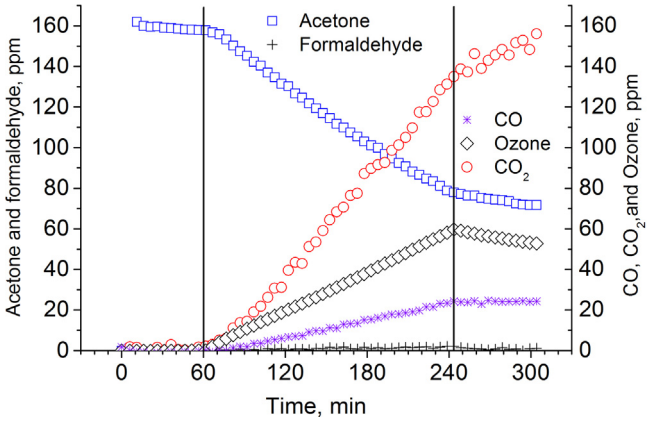

Fig. 8. Kinetics of acetone vapor oxidation with post-plasma TiO_2.

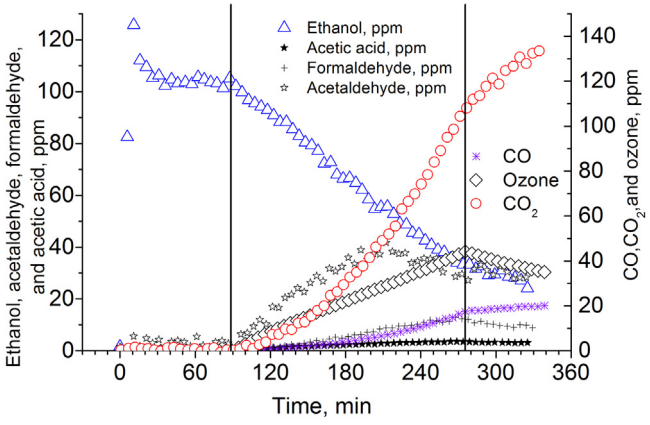

Fig. 9. Kinetics of ethanol vapor oxidation with post-plasma TiO_2.

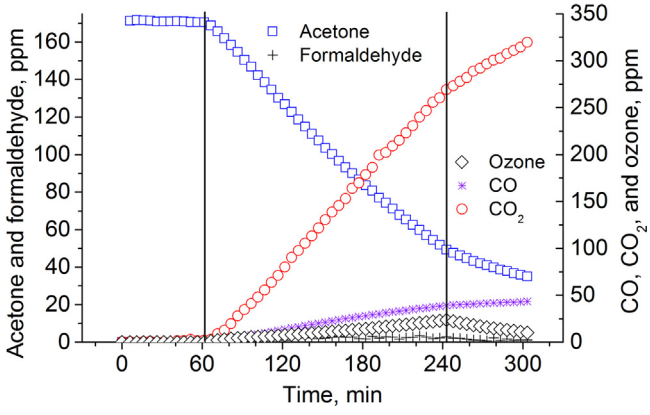

Fig. 10. Kinetics of acetone vapor oxidation with post-plasma MnO_2/TiO_2.

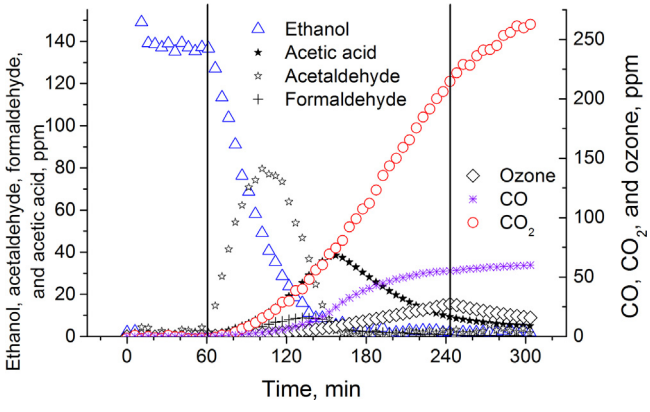

Fig. 11. Kinetics of ethanol vapor oxidation with post-plasma MnO_2/TiO_2.

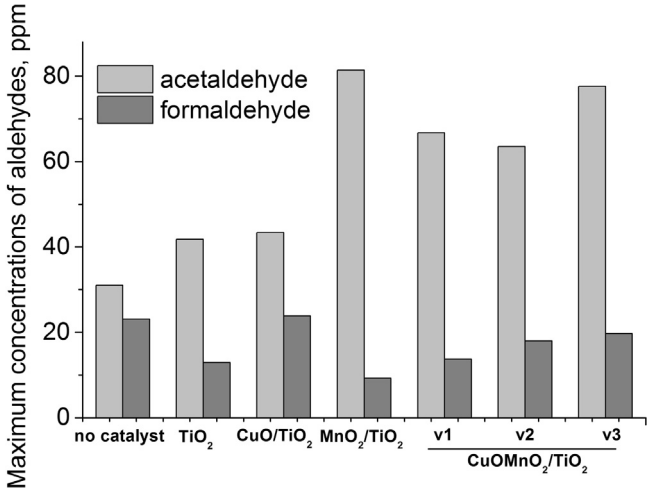

Fig. 12. Maximum concentrations of aldehyde during PPC oxidation of ethanol.

a chemical transformation scheme. First, ethanol transforms into acetaldehyde

$CH_3CH_2OH \rightarrow CH_3CHO.$

After that, there are two possible ways for the further oxidation: direct formation of formaldehyde from acetaldehyde (with the subsequent oxidation to formic acid and carbon oxides)

$CH_3CHO \rightarrow HCHO \rightarrow HCOOH \rightarrow CO_x$

or formation of formaldehyde through the formation of acetic acid

$CH_3CHO \rightarrow CH_3COOH \rightarrow HCHO \rightarrow HCOOH \rightarrow CO_x.$

Acetaldehyde and formaldehyde are the intermediates in the ethanol oxidation, and their maximum concentrations depend on the chemical transformation pathway. Previously, it was shown that they do not depend on parameters of a corona discharge [15]. Therefore, the relation of their maximum concentrations may reveal some changes in the reaction pathway when the oxidation is carried out using ozone decomposition catalysts in the post-plasma position. The obtained maximum concentrations of acetaldehyde and formaldehyde are presented in Fig. 12. As seen from the picture, the maximums obtained over the studied catalysts differ from those detected in the non-catalytic NTP oxidation. The concentrations of acetaldehyde became higher as a result of a faster initial step of the oxidation. The increase in the maximum concentration of acetaldehyde is rather related with the decrease in the concentration of formaldehyde: a more active catalyst promotes the oxidation of HCHO. The only case when the maximum concentration of formaldehyde remained at the constant level was the experiment with the CuO/TiO_2 sample.

The high concentrations of acetaldehyde indicate the rise of its generation rate as the first intermediate of the ethanol oxidation. The fall of maximum concentrations of formaldehyde shows an enhanced formaldehyde oxidation. Thus, our Mn-containing catalysts sufficiently enhance the oxidation of formaldehyde with ozone, which agrees well with published data [24].

3.4. Energy costs of acetone and ethanol decomposition

Energy efficiency is an important aspect for the characterization of electrically powered processes. Nevertheless, there is no universal parameter to evaluate energy costs of processes with plasma. The most widely used parameters for this purpose are Energy Cost (EC) and Energy Yield (EY) [4]. For fast estimations, the follow-

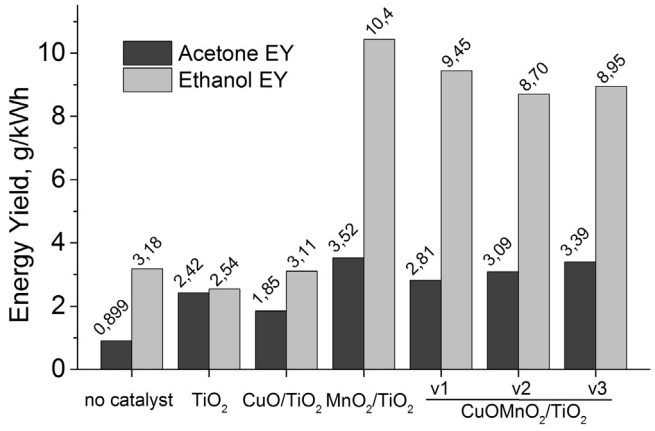

Fig. 13. Characteristic Energy Yields of acetone and ethanol decomposition in the non-catalytic plasma oxidation and in the oxidation with different post-plasma catalysts.

ing simple equations based on the consumption rate R and the discharge power P may be used:

$$\text{Energy Cost}\left[\frac{\text{eV}}{\text{molecule}}\right] = K_{EC} \times \frac{P\,[\text{W}]}{R\left[\frac{\text{ppm}}{\text{min}}\right]},$$

$$\text{Energy Yield}\left[\frac{\text{g}}{\text{kWh}}\right] = K_{EY} \times \frac{M_a\left[\frac{\text{g}}{\text{mol}}\right] \times R\left[\frac{\text{ppm}}{\text{min}}\right]}{P\,[\text{W}]},$$

where M_a is the molecular weight of a compound and K_{EC} and K_{EY} are conversion factors, calculated with Avogadro constant N_a, molar volume V_m, and chamber volume V:

$$K_{EC} = \frac{V_m}{N_a \times V} = 34.7\frac{\text{eV} \times \text{ppm}}{\text{molecule} \times W \times \text{min}},$$

$$K_{EY} = \frac{V}{V_m} = 1.08\frac{W \times \text{min} \times \text{mol}}{\text{kWh} \times \text{ppm}}.$$

A possible drawback of these equations is ignoring of reactant adsorption and of the variability of consumption rate. Indeed, the adsorption can significantly affect the oxidation of ethanol with TiO_2. Therefore, the neglect of the mass of adsorbed VOC can possibly lead to wrong estimations.

To obtain adequate estimations of total energy costs, we calculated the EY with taking into account both "gas" and "surface" portions of vapors. The amount of an adsorbed reactant was calculated in agreement with the Langmuir adsorption model on the basis of preliminary obtained isotherms of adsorption. The obtained EYs for both acetone and ethanol are shown on the histogram in Fig. 13. High rates of the ethanol decomposition with MnO_2-containing samples forced us to calculate the corresponding values from the results obtained at 1 h of discharge operation.

As seen from Fig. 13, the use of MnO_2-containing catalysts allows one to cut the energy cost of substrate decomposition by a factor of over 3 in comparison with non-catalytic NTP oxidation. Copper oxide as an active agent does not cause significant changes in the costs of acetone and ethanol decomposition as compared with TiO_2 as a post-plasma catalyst. Nevertheless, the use of pure titanium dioxide as a post-plasma catalyst can result in a decrease in the EY compared with the non-catalytic case. This is a result of the removal of VOC molecules from the volume exposed to plasma via their adsorption on a surface of TiO_2.

Concluding remarks

- Six different samples containing Cu, Mn, and TiO_2 were prepared and tested as ozone decomposition catalysts in the oxidation of acetone and ethanol.
- It was shown that the use of some of the catalysts can significantly reduce the concentration of ozone and accelerate the destruction of the test substances. The maximum decomposition rate, which was obtained for the MnO_2/TiO_2 sample, exceeds the rate achieved in non-catalytic plasma decomposition by more than 3 times.
- The order of oxide deposition does not significantly affects the activity of resulting $CuOMnO_2/TiO_2$ samples.
- Copper oxide as an active agent does not significantly change the effect of the TiO_2 presence in the post-plasma position. This is unexpected and slightly different from literature data.
- The use of post-plasma located catalysts can significantly improve the energy efficiency of air purifiers at no additional cost of electricity.

Acknowledgements

Help of Dr. D.A. Yatsenko, A.A. Saraev, and A.V. Ishchenko in obtaining XRD, XPS and TEM data is gratefully appreciated. We gratefully acknowledge the financial support for this work by the Russian Federal Department of Science and Education via the Federal Target Program "Scientific and Educational Personnel" contract 8440 as well as President Grant for the Leading Scientific Schools NSh 1183.2014.3.

The work was partially supported by base budget project V.44.2.11 and by the Skolkovo Foundation (Grant Agreement for Russian educational organization No. 3 on 25.12.2014).

References

[1] F.I. Khan, A. Kr Ghosal, J. Loss Prev. Proc. Ind. 13 (6) (2000) 527–545.
[2] T. Yamamoto, M. Okubo, Advanced Physicochemical Treatment Technologies: Handbook of Environmental Engineering, vol. 5, Humana Press, 2007, pp. 135–293.
[3] J.S. Chang, Plasma Sources Sci. Technol. 17 (4) (2008), 045004.
[4] H.H. Kim, Plasma Proc. Polym. 1 (2) (2004) 91–110.
[5] H.L. Chen, H.M. Lee, S.H. Chen, M.B. Chang, S.J. Yu, S.N. Li, Environ. Sci. Technol. 43 (2009) 2216–2227.
[6] A.M. Vandenbroucke, R. Morent, N. De Geyter, C. Leys, J. Hazard. Mater. 195 (2011) 30–54.
[7] A.V. Vorontsov, M.N. Lyulyukin, A.S. Besov, Global J. Environ. Sci. Technol. 2 (3) (2012) 1–10.
[8] F. Holzer, U. Roland, F.D. Kopinke, Appl. Catal. B: Environ. 38 (3) (2002) 163–181.
[9] Ch. Subrahmanyam, M. Magureanu, A. Renken, L. Kiwi-Minsker, Appl. Catal. B: Environ. 1-2 (2006) 150–156.
[10] S.T. Oyama, W. Li, W. Zhang, Stud. Surf. Sci. Catal. 121 (1999) 105–110.
[11] Y. Xi, C. Reed, Y.K. Lee, S.T. Oyama, J. Phys. Chem. B 109 (37) (2005) 17587–17596.
[12] J. Van Durme, J. Dewulf, W. Sysmans, C. Leys, H. Van Langenhove, Appl. Catal. B 1-2 (2007) 161–169.
[13] A. Naydenov, D. Mehandjiev, Appl. Catal. A 97 (1) (1993) 7–22.
[14] M.N. Lyulyukin, A.S. Besov, A.V. Vorontsov, Plasma Chem. Plasma Proc. 31 (1) (2011) 23–39.
[15] M.N. Lyulyukin, A.S. Besov, A.V. Vorontsov, Ind. Eng. Chem. Res. 52 (17) (2013) 5842–5848.
[16] D. Kozlov, A. Besov, Appl. Spectrosc. 65 (8) (2011) 918–923.
[17] J.H. Scofield, J. Electron Spectrosc. Relat. Phenom. 8 (2) (1976) 129–137.
[18] D.A. Shirley, Phys. Rev. B 5 (12) (1972) 4709–4714.
[19] CasaXPS. Processing Software for XPS, AES, SIMS and More. http://www.casaxps.com (accessed 07.04.15).
[20] E. Regan, T. Groutso, J.B. Metson, R. Steiner, B. Ammundsen, D. Hassell, P. Pickering, Surf. Interface Anal. 27 (12) (1999) 1064–1068.
[21] J.S. Foord, R.B. Jackman, G.C. Allen, Philos. Mag. A 49 (5) (1984) 657–663.
[22] Ch. Subrahmanyam, Indian J. Chem. 48A (2009) 1062–1068.
[23] S.T. Oyama, Catal. Rev. Sci. Eng. 42 (3) (2000) 279–322.
[24] D.Z. Zhao, C. Shi, X.S. Li, A.M. Zhu, B.W. Jang, J. Hazard. Mater. 239-240 (2012) 362–369.